J Mater Sci: Mater Med (2011) 22:2599–2605
DOI 10.1007/s10856-011-4443-z

Analysis of sintered polymer scaffolds using concomitant synchrotron computed tomography and in situ mechanical testing

A. Dhillon · P. Schneider · G. Kuhn · Y. Reinwald · L. J. White · A. Levchuk · F. R. A. J. Rose · R. Müller · K. M. Shakesheff · C. V. Rahman

Received: 27 July 2011 / Accepted: 29 August 2011 / Published online: 10 September 2011
© Springer Science+Business Media, LLC 2011

Abstract The mechanical behaviour of polymer scaffolds plays a vital role in their successful use in bone tissue engineering. The present study utilised novel sintered polymer scaffolds prepared using temperature-sensitive poly(DL-lactic acid-*co*-glycolic acid)/poly(ethylene glycol) particles. The microstructure of these scaffolds was monitored under compressive strain by image-guided failure assessment (IGFA), which combined synchrotron radiation computed tomography (SR CT) and in situ micro-compression. Three-dimensional CT data sets of scaffolds subjected to a strain rate of 0.01%/s illustrated particle movement within the scaffolds with no deformation or cracking. When compressed using a higher strain rate of 0.02%/s particle movement was more pronounced and cracks between sintered particles were observed. The results from this study demonstrate that IGFA based on simultaneous SR CT imaging and micro-compression testing is a useful tool for assessing structural and mechanical scaffold properties, leading to further insight into structure–function relationships in scaffolds for bone tissue engineering applications.

A. Dhillon · Y. Reinwald · L. J. White · F. R. A. J. Rose · K. M. Shakesheff · C. V. Rahman (✉)
Division of Drug Delivery and Tissue Engineering, Centre for Biomolecular Sciences, University of Nottingham, University Park, Nottingham NG7 2RD, UK
e-mail: cheryl.rahman@nottingham.ac.uk

P. Schneider · G. Kuhn · A. Levchuk · R. Müller
Institute for Biomechanics, ETH Zurich, Wolfgang-Pauli-Strasse 10, 8093 Zurich, Switzerland

1 Introduction

The contribution of the microstructure of bone to its mechanical properties is widely accepted [1, 2]. For instance, it has been shown that for trabecular bone the mechanical properties depend on the morphology and distribution of the individual trabeculae [3]. Such knowledge of the biomechanical properties of trabecular bone is necessary and relevant to obtain insight into the design and analysis of scaffolds for bone repair. While scaffolds made from synthetic or natural polymers have excellent potential for use in this area, an ideal scaffold for bone tissue engineering requires a number of specific properties, including appropriate mechanical strength and microstructure [4–6]. In general, the scaffold must be strong enough to retain its structure in a load bearing environment after implantation, yet without exhibiting stiffness that could cause the surrounding bone to be shielded from load [7]. In addition, mechanical properties are strongly influenced by the internal microstructure of the scaffold [8]. Therefore, scaffolds for bone regeneration must be carefully designed to exhibit structural and mechanical properties which match that of the host bone as closely as possible. Moreover, the microstructure plays a pivotal role in bone repair as it determines the rate and degree of bone ingrowth [9, 10]. Consequently, the requirement for a thorough characterisation of scaffold structural and mechanical properties is crucial in order to assess their suitability for bone tissue engineering.

The mechanical properties of scaffolds are generally measured by way of their compressive strength, as this is considered to be one of the main loading modes they will be subjected to in vivo [11]. However, methods used to assess compressive strength alone do not allow concurrent visualisation of scaffold microstructure under strain along

with compression analysis. Following the changes in scaffold microstructure as strain increases could provide valuable information to assist scaffold design for bone tissue engineering applications. Computed tomography (CT) is an ideal imaging method to investigate the behaviour of a porous structure, such as a polymer scaffold, under compression and at spatial resolutions in the micrometer range. Compression testing in specially designed rigs that fit inside the CT allows simultaneous imaging of the internal scaffold microstructure while obtaining mechanical data. This image-guided failure assessment (IGFA) approach has been effectively used to investigate deformation and failure in metallic structural materials and polyurethane foam [12, 13]. Further, an in situ mechanical compression device (MCD) was used to perform IGFA for the non-destructive imaging of bone deformation at different time points during the failure process [14, 15]. New generations of MCDs have been developed and used in the same group in conjunction with synchrotron radiation (SR) CT to successfully visualise microcrack initiation and propagation in bone tissue [16–18].

In this study, we were especially interested in the combination of SR CT with micro-compression testing to gain new insights into the behaviour of poly(DL-lactic acid-*co*-glycolic acid)/poly(ethylene glycol) (PLGA/PEG) particles within a sintered scaffold under compressive strain. PLGA has been used for a number of years as an implant material, due to advantages including biodegradability, biocompatibility and the fact that products containing PLGA have been approved by regulatory authorities around the world for certain clinical applications [19, 20]. Blending PLGA with a plasticiser, such as PEG, results in production of temperature-sensitive particles with a reduced glass transition temperature (T_g) of 37°C [21]. When the PLGA/PEG particles are mixed with a carrier solution at room temperature, a particulate paste is formed that can be injected or moulded into any size or shape. The paste then hardens into a scaffold at 37°C due to heat sintering. During this process the particles becoming soft and cohesive when they reach their T_g and adhere to each other. At this stage, the hydrophilic PEG component starts to leach out of the particles resulting in a decrease in PEG concentration. This leads to an increase in the T_g of the particles, causing them to re-solidify forming porous, strong scaffolds.

In the present study, the microstructure of PLGA/PEG sintered scaffolds was analysed using IGFA by combining SR CT and in situ micro-compression. To our knowledge this is the first report on the use of SR CT-based IGFA to investigate structure–function relationships in particulate polymer scaffolds for bone tissue engineering.

2 Materials and methods

2.1 PLGA/PEG particle production

Thermosensitive particles were fabricated from blends of 53 kDa P_{DL}LGA (85:15 DLG 4CA) (Lakeshore Biomaterials, USA) and PEG 400 (Sigma Aldrich, UK). A mixture of 93.5:6.5% PLGA:PEG (*w/v*) was blended at 80–90°C on a hotplate. The melted PLGA and PEG were mixed together by hand using a polytetrafluoroethylene (PTFE)-coated spatula and the mixture was allowed to cool to room temperature. Polymer blend sheets were then ground into particles in a bench-top mill (Krups Mill F203) and the particles were sieved to obtain the 100–200 μm particle size fraction.

2.2 Scaffold preparation

Triplicate scaffolds were prepared in PTFE moulds producing cylindrical scaffolds of 12 mm length and 6 mm diameter which fitted into the MCD. The PLGA/PEG particles were mixed manually with saline solution. A ratio of 1:0.6 of particles to solution was used. The particle paste was then packed into the mould which was placed at 37°C for 2 h to allow scaffold formation.

2.3 Scanning electron microscopy

Samples were mounted on aluminium stubs and were sputter-coated with gold at an argon current rate of 30 mA for 3 min. The structural morphology of the scaffolds was visualised using a scanning electron microscope (SEM) (JEOL JSM-6060LV) at 10 kV.

2.4 Mechanical testing

Compressive strength of the PLGA/PEG scaffolds was tested using a TA.HD+ texture analyser (Stable Microsystems, UK) with a Peltier unit heated to 37°C and a scaffold contact area of 28.26 mm^2. A 50 kg load cell and P/10 probe were used for compression testing. The pre-test speed was set at 1 mm/s, test speed at 0.04 mm/s, and post-test speed at 10 mm/s. Strain was set at 30%. The compressive strength was recorded as the maximum stress at the yield point of the scaffold (the fracture peak).

2.5 IGFA using concomitant SR CT imaging and in situ mechanical testing

All tomography experiments were performed at the TOMCAT beamline of the Swiss light source (SLS) [22]. Between each loading set a high-resolution 3D data set was acquired using SR CT. The overall volume of interest

(VOI) assessed within the scaffolds was 1024 × 1024 × 1024 voxels or 1.5 × 1.5 × 1.5 mm^3. For each 3D data set 1,001 projections were acquired over a range of 180° at a photon energy of 13.5 keV. Images were reconstructed using filtered back projection, resulting in an isotropic voxel size of 1.48 μm. During reconstruction a filter was applied and a ring removal algorithm was active.

The in situ MCD is described elsewhere [18]. Each scaffold was placed into the sample chamber of the MCD and was imaged by SR CT prior to compression. Two different strain rates were used, 0.01 and 0.02%/s. The strain rate of 0.01%/s was chosen as it was previously used with the MCD and SR CT to assess trabecular bone failure [15]. The increased strain rate of 0.02%/s was selected in order to observe any differences in particle behaviour under higher strain. For the two different loading regimes at 0.01 and 0.02%/s strain rate, triplicate scaffolds were subjected to a preload of 1 or 2 N before testing, respectively. Ten compression steps were performed at a strain rate of 0.01%/s for a maximum of 10% strain and 0.02%/s for a maximum of 20% strain. This was an interrupted test as scans were carried out for 6 min after each compression step to obtain the CT data. Each compression step took 100 s, with 120 s relaxation time between compression steps. Particle behaviour under both strain rates was assessed by visual inspection of 100 reconstructed slices for each scaffold.

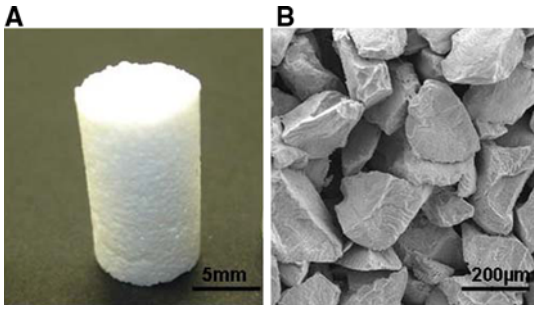

Fig. 1 PLGA/PEG scaffolds **a** Representative PLGA/PEG scaffolds fabricated by sintering 100–200 μm PLGA/PEG particles mixed with saline (ratio of 1.0:0.6 particles:saline) in Teflon moulds at 37°C for 2 h. **b** Microstructure of PLGA/PEG scaffold visualized by scanning electron microscopy (SEM)

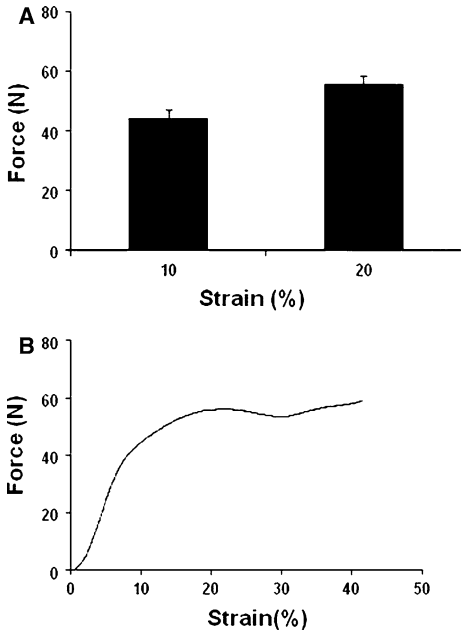

Fig. 2 Compressive strength of PLGA/PEG scaffolds. Compressive strength of scaffolds fabricated by sintering 100–200 μm PLGA/PEG particles mixed with saline (ratio of 1:0.6 particles:saline) in Teflon moulds at 37°C for 2 h was tested in a TA.HD+ texture analyser. **a** The force that scaffolds were subjected to, under 10 and 20% strain, was determined. *Error bars* represent SD. **b** Representative compression trace up to 50% strain

3 Results

3.1 Compressive strength of PLGA/PEG scaffolds

PLGA/PEG scaffolds were produced by mixing 100–200 μm PLGA/PEG particles with saline and sintering in Teflon

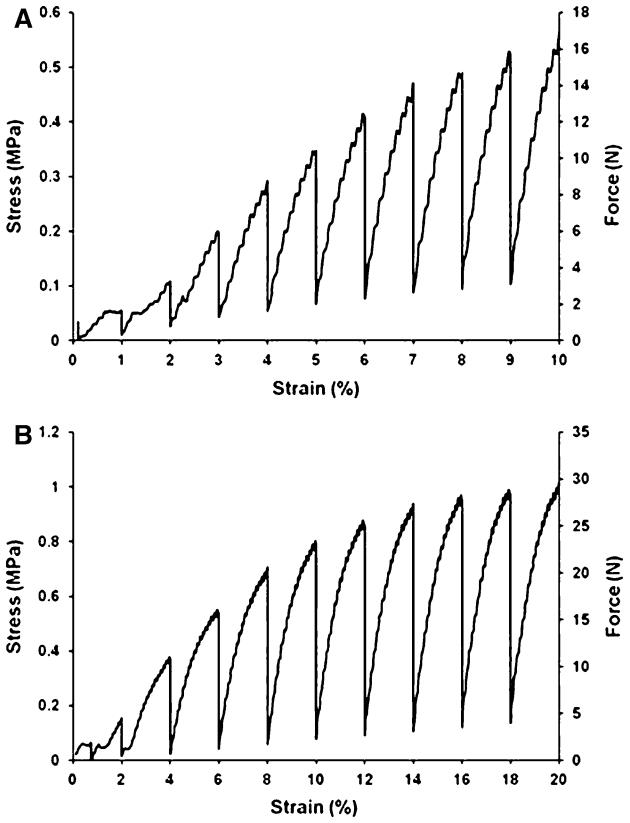

Fig. 3 Compression of PLGA/PEG scaffolds using the in situ mechanical compression device (MCD) integrated inside the synchrotron CT setup. **a** 10 compression steps were performed at a strain rate of 0.01%/s for a maximum of 10% strain and **b** 0.02%/s for a maximum of 20% strain

moulds at 37°C for 2 h (Fig. 1). The compressive strength of triplicate PLGA/PEG scaffolds was tested using a TA.HD+ texture analyser. At 10% strain the scaffolds were subjected to a force of approximately 45 N on average (Fig. 2a). Scaffolds typically fractured at 20% strain under a force of approximately 56 N, corresponding to a stress of 2 MPa (Fig. 2b).

3.2 IGFA of PLGA/PEG scaffolds

Continuous mechanical tests were performed on the PLGA/PEG scaffolds using the in situ MCD integrated within the SR CT setup. Ten compression steps were performed at a strain rate of 0.01%/s for a maximum of 10% strain and 0.02%/s for a maximum of 20% strain (Figure 3). For each strain rate the increasing force is plotted as assessed during the individual compression steps and CT data sets were taken after each compression step. During imaging the displacement was fixed and a sharp decrease in force was observed in the load–displacement curves, which represents scaffold relaxation during the time between two successive loading steps, where force data was not recorded.

3.3 Analysis of the microstructure of PLGA/PEG scaffolds under strain

Reconstructed CT data of the scaffolds for each compression step illustrated the position of the PLGA/PEG microparticles within the scaffolds. Over each compression step it was possible to track particular areas within the scaffolds by visual assessment of the reconstructed slices, allowing the particle behaviour and changes in microstructure under strain to be observed. Movement of particles under compression in scaffolds that experienced a strain rate of 0.01 or 0.02%/s was observed. Particles could be observed 'sintering' (merging with other particles) over compression steps in scaffolds that were subjected to the lower strain rate of 0.01%/s, due to the combined effects of the increased temperature in the synchrotron beam (approximately 26°C) and the low compressive forces (Fig. 4). No particle sintering was observed at the higher

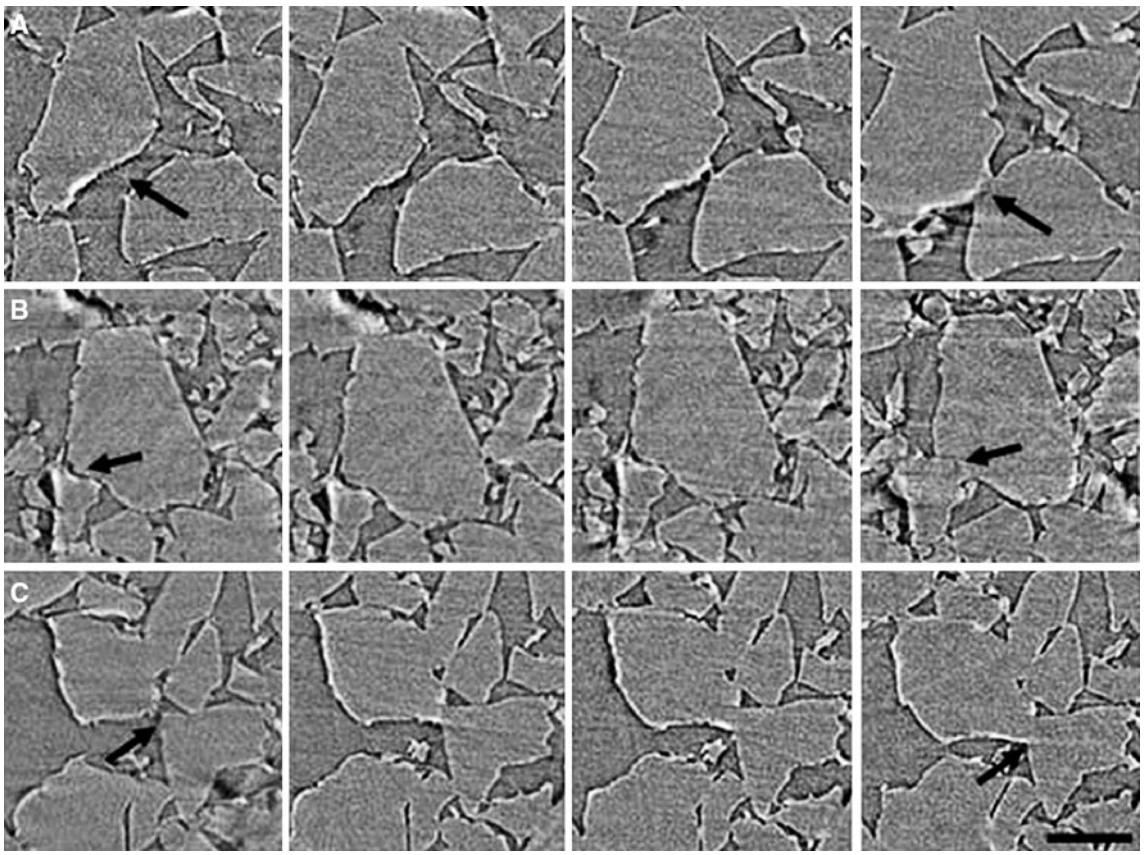

Fig. 4 Reconstructed slices of PLGA/PEG scaffolds subjected to 0.01% strain. **a**, **b**, **c** Representative slice images are shown for each of the three scaffolds tested. Scaffolds were subjected to a strain rate of 0.01%/s with a maximum of 10% strain. Increased strain is shown in images from left to right. Arrows indicate areas of particle sintering. Data has been assessed using synchrotron CT at 1.48 μm nominal resolution. Size bar represents 100 μm

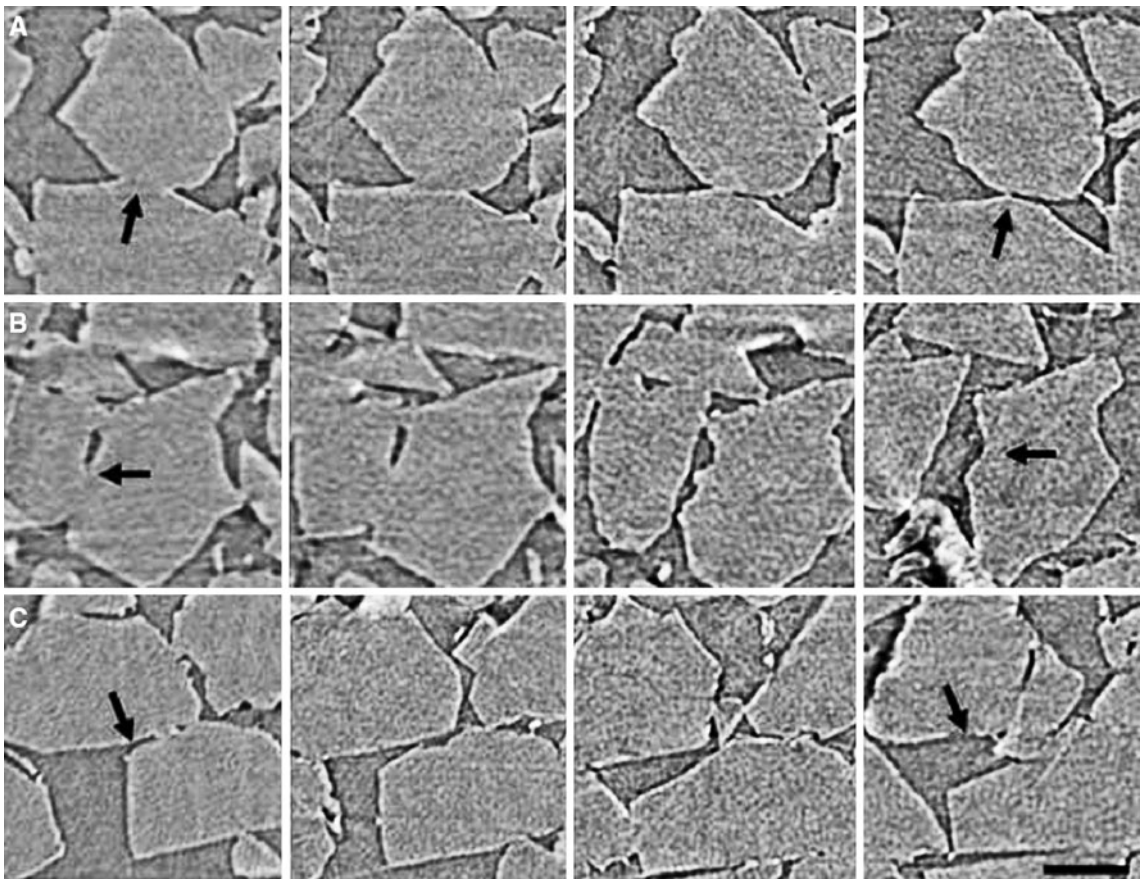

Fig. 5 Reconstructed slices of PLGA/PEG scaffolds subjected to 0.05% strain. **a**, **b**, **c** Representative slice images are shown for each of the three scaffolds tested. Scaffolds were subjected to a strain rate of 0.02%/s with a maximum strain of 20%. Increased strain is shown in images from *left to right*. *Arrows* indicate areas where cracks appeared between particles. Data has been assessed using synchrotron CT at 1.48 μm nominal resolution. *Size bar* represents 100 μm

strain rate of 0.02%/s with a maximum strain of 20%. Under this strain rate (0.02%/s) cracks appeared between particles that had previously sintered together during scaffold formation. Visual assessment of reconstructed images from subsequent compressive steps allowed observation of these cracks widening, causing the particles to break apart and move away from each other due to the increased compressive strain (Fig. 5).

4 Discussion

In this study PLGA/PEG sintered scaffolds were analysed under compressive strain using IGFA, which combined SR CT with in situ mechanical compression. The mechanical behaviour and microstructure of scaffolds play a pivotal role for their successful use in bone tissue engineering. It is vital that scaffolds exhibit adequate compressive strength, preferably mimicking the strength of host bone. The strength of trabecular bone varies at different sites in the human body, ranging from 0.22 MPa in the mandible to 10.4 MPa in the spine [23, 24]. The results from this study demonstrate that PLGA/PEG scaffolds sintered at 37°C for 2 h have a compressive strength of 2 MPa when tested using a laboratory texture analyser. The compressive strength of the PLGA/PEG scaffolds therefore falls within the range for human trabecular bone, and demonstrates their suitability for use as scaffolds in bone tissue engineering applications.

The PLGA/PEG scaffolds were imaged concomitantly using SR CT with the applied loading regime in the in situ MCD, which allowed comparison between images obtained after each compression step and observation of changes in particle position and morphology regarding the overall compressive strain. For both strain rates tested (0.01 and 0.02%/s) the particles were observed to move within the scaffolds under compression by visual inspection of the reconstructed slices for each scaffold, however, movement was more pronounced under the higher strain rate of 0.02%/s. Particles were observed 'sintering' in the scaffolds subjected to the low strain rate of 0.01%/s, thought to be due to the combined effects of the low level

of compression and the temperature in the beam line of approximately 26°C. Sintered particles were observed cracking under compression when subjected to the higher strain rate. Visual inspection of reconstructed slices for each scaffold showed that the cracks increased in size and particles separated as strain increased. Trabecular bone has been reported to demonstrate similar behaviour under compression, with each individual trabecula 'buckling' (collapsing) [25].

SR CT in conjunction with an MCD has previously been utilised to visualise microcrack propagation in trabecular and cortical bone [16, 17]. Interactions between microcracks and microscopic bone structures were identified using this method. SR CT has also been combined with in situ mechanical testing for mechanical and structural characterisation of PLA-calcium phosphate glass composite scaffolds and bioactive glass scaffolds [26, 27].

To our knowledge, this is the first report on concomitant SR CT and in situ mechanical testing for investigation of sintered polymer scaffolds under compression. This biomechanical imaging approach was used in this study to successfully visualise the microstructure and behaviour of PLGA/PEG sintered scaffolds under compressive strain.

5 Conclusion

SR CT combined with in situ mechanical compression allowed investigation of scaffold properties under strain, particularly the interaction between the particles within the scaffolds. This study demonstrated that a difference in strain rate during compression caused changes in particle behaviour. Cracks were observed to appear only between sintered particles in scaffolds subjected to the higher strain rate of 0.02%/s. In conclusion, SR CT used in conjunction with in situ mechanical compression has the potential to provide further insight into structural and mechanical properties of scaffolds for bone tissue engineering applications.

Acknowledgments This study has benefited from research funding of the European Union's access programme 20090893 at the SLS (Paul Scherrer Institut, Villigen, Switzerland) as well as from the European Union's Seventh Framework Programme in the project Angioscaff NMP-LA-2008-214402. SR CT measurements were carried out at the TOMCAT beamline at the Swiss Light Source with assistance from Dr Julie Fife. The authors also acknowledge Dr Kathryn Stok for her help and advice.

References

1. Mosekilde L. Age-related changes in vertebral trabecular bone architecture—assessed by a new method. Bone. 1988;9:247–50.
2. Müller R, Hannan M, Smith SY, Bauss F. Intermittent ibandronate preserves bone quality and bone strength in the lumbar spine after 16 months of treatment in the ovariectomized cynomolgus monkey. J Bone Miner Res. 2004;19:1787–96.
3. Goulet RW, Goldstein SA, Ciarelli MJ, Kuhn JL, Brown MB, Feldkamp LA. The relationship between the structural and orthogonal compressive properties of trabecular bone. J Biomech. 1994;27:375–89.
4. Langer R, Vacanti JP. Tissue engineering. Science. 1993;260:920–6.
5. Salgado AJ, Coutinho OP, Reis RL. Bone tissue engineering: state of the art and future trends. Macromol Biosci. 2004;4:743–65.
6. Jones JR, Lee PD, Hench LL. Heirarchical porous materials for tissue engineering. Philos Transact A Math Phys Eng Sci. 2006;364:263–81.
7. Yang S, Leong KF, Du Z, Chua CK. The design of scaffolds for use in tissue engineering. Part I. Tradit Factors. 2001;7:679–89.
8. Bignon A, Chouteau J, Chevalier J, Fantozzi G, Carret JP, Chavassieux P, Boivin G, Melin M, Hartmann D. Effect of micro- and macroporosity of bone substitutes on their mechanical properties and cellular response. J Mater Sci Mater Med. 2003;14:1089–97.
9. Jin QM, Takita H, Kohgo T, Atsumi K, Itoh H, Kuboki Y. Effects of geometry of hydroxyapatite as a cell substratum in BMP-induced ectopic bone formation. J Biomed Mater Res A. 2000;51:491–9.
10. Kaito T, Myoui A, Takaoka K, Saito N, Nishikawa M, Tamai N, Ohgushi H, Yoshikawa H. Potentiation of the activity of bone morphogenetic protein-2 in bone regeneration by a PLA/PEG/hydroxyapatite composite. Biomaterials. 2005;26:73–9.
11. Marra KG, Szem JW, Kumta PN, DiMilla PA, Weiss LE. In vitro analysis of biodegradable polymer blend/hydroxyapatite composites for bone tissue engineering. J Biomed Mater Res. 1999;47:324–35.
12. Babout L, Ludwig W, Maire E, Buffiere JY. Damage assessment in metallic structural materials using high resolution synchrotron X-ray tomography. Nucl Instrum Methods Phys Res, B Beam Interact Mater Atoms. 2003;200:303–7.
13. Elliott JA, Windle AH, Hobdell JR, Eeckhaut G, Oldman RJ, Ludwig W, Boller E, Cloetens P, Baruchel J. In situ deformation of an open-cell flexible polyurethane foam characterised by 3D computed microtomography. J Mater Sci. 2002;37:1547–55.
14. Müller R, Gerber SC, Hayes WC. Micro-compression: a novel technique for the non-destructive assessment of local bone failure. Technol Health Care. 1998;6:433–44.
15. Nazarian A, Müller R. Time-lapsed microstructural imaging of bone failure behaviour. J Biomech. 2004;37:55–65.
16. Thurner PJ, Wyss P, Voide R, Stauber M, Stampanoni M, Sennhauser U, Müller R. Time-lapsed investigation of three-dimensional failure and damage accumulation in trabecular bone using synchrotron light. Bone. 2006;39:289–99.
17. Voide R, Schneider P, Stauber M, Wyss P, Stampanoni M, Sennhauser U, van Lenthe GH, Müller R. Time-lapsed assessment of microcrack initiation and propagation in murine cortical bone at submicrometer resolution. Bone. 2009;45:164–73.
18. Schneider P, Levchuk A, Müller R. Automated micro-compression device for dynamic image-guided failure assessment of bone ultrastructure and bone microdamage. Biomed Tech. 2010;55:8–10.
19. Coombes AG, Heckman JD. Gel casting of resorbable polymers 2. In vitro degradation of bone graft substitutes. Biomaterials. 1992;13:297–307.
20. Howard D, Buttery LD, Shakesheff KM, Roberts SJ. Tissue engineering: strategies, stem cells and scaffolds. J Anat. 2008;213:66–72.
21. Hamilton L, France RM, Shakesheff KM. Development of an injectable scaffold for application in regenerative medicine to

deliver stem cells and growth factors. J Pharm Pharmacol. 2006;58:52–3.
22. Stampanoni M, Groso A, Isenegger A, Mikuljan G, Chen Q, Meister D, Lange M, Betemps R, Henein S, Abela R. TOMCAT: a beamline for tomographic microscopy and coherent radiology experiments. AIP Conf Proc. 2007;879:848–51.
23. Misch CE, Qu Z, Bidez MW. Mechanical properties of trabecular bone in the human mandible: implications for dental implant treatment planning and surgical placement. J Oral Maxillofac Surg. 1999;57:700–6.
24. Teo JC, Chui CK, Wang ZL, Ong SH, Yan CH, Wang SC, Wong HK, Teoh SH. Heterogenous meshing and biomechanical modelling of human spine. Med Eng Phys. 2007;29:277–90.
25. Kopperdahl DL, Keaveny TM. Yield strain behaviour of trabecular bone. J Biomech. 1998;31:601–8.
26. Charles-Harris M, del Valle S, Hentges E, Bleuet P, Lacroix D, Planell JA. Mechanical and structural characterisation of completely degradable polylactic acid/calcium phosphate glass scaffolds. Biomaterials. 2007;28:4429–38.
27. Yue S, Lee PD, Poologasundarampillai G, Yao Z, Rockett P, Devlin AH, Mitchell CA, Konerding MA, Jones JR. Synchrotron X-ray microtomography for assessment of bone tissue scaffolds. J Mater Sci Mater Med. 2010;21:847–53.